NWC TP 6846

Terminal Shock Response in Ramjet Inlets to Abrupt Downstream Perturbations

by

M. Sajben
T. J. Bogar
McDonnell Douglas Research Laboratories

for
Ordnance Systems Department

SEPTEMBER 1988

NAVAL WEAPONS CENTER
CHINA LAKE, CA 93555-6001

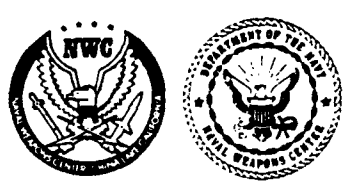

Approved for public release; distribution unlimited.

Naval Weapons Center

FOREWORD

This final report summarizes the results of a research program performed by the McDonnell Douglas Research Laboratories (MDRL), St. Louis, Missouri, on the response of ramjet inlets to abrupt downstream perturbations. The research was conducted for the Naval Weapons Center (NWC), China Lake, California, under Contract No. N60530-83-C-0186. The performance period was 1 October 1983 to 30 June 1987.

This work was performed in the Flight Sciences Department of MDRL under the supervision of Dr. Raimo J. Hakkinen. The principal investigator was Dr. Miklos Sajben; Dr. Thomas J. Bogar and Mr. Joseph C. Kroutil were co-investigators. The report was reviewd and approved at MDRL by Dr. Hakkinen and by D. P. Ames, general manager, MDRL.

The initial program manager at NWC was Dr. William H. Clark. He was succeeded in 1985 by Mr. C. F. Markarian, also of NWC, who has reviewed this report for technical accuracy. It is released for information and does not necessarily reflect the views of NWC.

In the interest of saving time and cost, this report is being reprinted as submitted by MDRL. Consequently, it does not conform in all formatting details to standard NWC report requirements.

Approved by
M. E. ANDERSON, *Head*
Ordnance Systems Department
30 September 1988

Under authority of
J. A. BURT
Capt., USN
Commander

Released for publication by
G. R. SCHIEFER
Technical Director

NWC Technical Publication 6846

Published by . . . . . Technical Information Department
Collation . . . . . Cover, 22 leaves
First printing . . . . . 228 copies

REPORT DOCUMENTATION PAGE

1a. REPORT SECURITY CLASSIFICATION UNCLASSIFIED	1b. RESTRICTIVE MARKINGS
2a. SECURITY CLASSIFICATION AUTHORITY	3. DISTRIBUTION/AVAILABILITY OF REPORT Approved for public release; distribution unlimited
2b. DECLASSIFICATION/DOWNGRADING SCHEDULE	
4. PERFORMING ORGANIZATION REPORT NUMBER(S) MDC Q1285	5. MONITORING ORGANIZATION REPORT NUMBER(S) NWC TP 6846
6a. NAME OF PERFORMING ORGANIZATION McDonnell Douglas Research Labs McDonnell Douglas Corporation 6b. OFFICE SYMBOL (If Applicable)	7a. NAME OF MONITORING ORGANIZATION Naval Weapons Center
6c. ADDRESS (*City, State, and ZIP Code*) P. O. Box 516, 222/110/1/MS1 St. Louis, MO 63166	7b. ADDRESS (*City, State, and ZIP Code*) China Lake, CA 93555-6001
8a. NAME OF FUNDING/SPONSORING ORGANIZATION Naval Weapons Center 8b. OFFICE SYMBOL (If Applicable)	9. PROCUREMENT INSTRUMENT IDENTIFICATION NUMBER Contract No. N60530-83-C-0186
8c. ADDRESS (*City, State, and ZIP Code*) China Lake, CA 93555-6001	10. SOURCE OF FUNDING NUMBERS PROGRAM ELEMENT NO. / PROJECT NO. / TASK NO. / WORK UNIT

11 TITLE (*Include Security Classification*)

Terminal Shock Response in Ramjet Inlets to Abrupt Downstream Perturbations (U)

12 PERSONAL AUTHOR(S)

Sajben, M.; Bogar, T. J.

13a TYPE OF REPORT	13b. TIME COVERED	14. DATE OF REPORT (Year, Month, Day)	15. PAGE COUNT
	From 9/29/83 To 6/30/87	1988, September	42

16. SUPPLEMENTARY NOTATION

17. COSATI CODES			18. SUBJECT TERMS (*Continue on reverse side if necessary and identify by block number*)
FIELD	GROUP	SUB-GROUP	Airbreathing propulsion; Flowfield oscillations; Internal flow; Laboratory simulation tests; Pressure fluctuations; Transonic flow; Two-dimensional model

19. ABSTRACT (*Continue on reverse side if necessary and identify by block number*)

(U) The response of a nominally two-dimensional transonic diffuser flow to abrupt downstream perturbations was examined experimentally. The objective was to separate the acoustic and convective waves responsible for the self-excited oscillations in transonic diffuser flows and to subject these waves to individual scrutiny. This objective was accomplished by initiating a fast-rise-time, ramp-type pulse at the downstream end of the flowfield.

(U) A novel device based on shock-tunnel principles was developed to introduce the disturbance. The requirements were a short (<0.1 ms) pulse rise time and a pulse duration sufficiently long for the pulse to

20. DISTRIBUTION/AVAILABILITY OF ABSTRACT ☐ UNCLASSIFIED/UNLIMITED ☐ SAME AS RPT. ☒ DTIC USERS	21. ASTRACT SECURITY CLASSIFICATION Unclassified
22a. NAME OF RESPONSIBLE INDIVIDUAL C. F. Markarian	22b. TELEPHONE (*Include Area Code*) 619-939-7395 22c. OFFICE SYMBOL 3246

Item 19 (contd.)

propagate upstream to the shock and for any reflections to propagate back downstream to the end of the diffuser. The conditions were either met or exceeded by the device.

(U) The response of the diffuser to the perturbation was investigated over a shock Mach-number range which included weak-shock ($1.18 < M_0 < 1.27$) and strong-shock ($1.27 < M_0 < 1.38$) flows. A study was also make of the effect of pulse strength for one weak-shock and one strong-shock flowfield. Static- and total-pressure core-flow mappings were made for these same two cases.

(U) The pulse injection created an upstream-traveling acoustic wave in both weak- and strong-shock flows. In the weak-shock case, this acoustic wave was the only disturbance observed. For the strong-shock case, the interaction of the acoustic wave with the normal shock at the upstream end of the subsonic flowfield caused a boundary layer disturbance which was convected downstream at a speed considerably lower than the core-flow speed.

(U) The initial pulse strength was varied over a 3:1 range for both weak- and strong-shock cases. Normalizing the pulse amplitudes measured over the length of the diffuser with the initial pulse strength resulted in a good correlation of the data for both cases.

(U) In a related IR&D effort, the characteristics determined for the individual elementary waves found in this study were used to reconstruct the composite wave propagation characteristics found in self-excited and periodically excited strong-shock diffuser flows. The reconstructions compared well with the experimental data, indicating that the elementary waves found in this study behave in the same manner as those existing in the strong-shock oscillations.

CONTENTS

1.0 INTRODUCTION

Large-amplitude, low-frequency pressure oscillations have been recognized as a major limiting factor in the performance of ramjet propulsion systems.[1-9] The oscillations arise from combustion instabilities occurring in the combustor, and from the inherent instability of the transonic diffuser in the inlet system. Coupling between these two systems can lead to unacceptably high pressure levels which degrade system performance, unstart the inlet, and cause structural failure.

McDonnell Douglas Research Laboratories (MDRL) has been examining inlet system unsteadiness through studies of the self-excited and externally excited flowfields in transonic diffusers.[10-17] The flowfields fall into three basic classes, as depicted in Fig. 1. The type of unsteadiness observed depends strongly on the type of mean flowfield which exists in the diffuser. Moderate-area-ratio diffusers with relatively weak shocks (Fig. 1a) contain fully attached flow with thin boundary layers. A well-defined core flow exists to the end of the diffuser. For weak shocks in large-area-ratio diffusers (Fig. 1b), a pressure-gradient-induced separation may occur. However, the boundary layers remain relatively thin. For all strong-shock flows, independent of area ratio (Fig. 1c), the flow exhibits a shock-induced separation. The boundary layers grow rapidly and merge within the diverging section, terminating the core flow.

Three fundamental mechanisms have been proposed as contributors to the observed unsteadiness[18] (Fig. 2): upstream and downstream-traveling acoustic waves, and a disturbance which is convected through a thick, separated boundary layer, such as depicted in Fig. 1c. The convective wave is generated by the recoil of the shock after impingement of an upstream-traveling acoustic wave.

A common method used to examine unsteady flowfields in a controlled manner is to subject the flow to a known, periodic excitation. This method has proven useful in the study of coherent structures in free shear layers and jets,[19-21] as well as in air-breathing propulsion systems.[22-23] This technique allows the overall response of the system to be measured. One advantage of periodic excitation methods is that they are relatively easily implemented. Their major shortcoming is that in cases where several

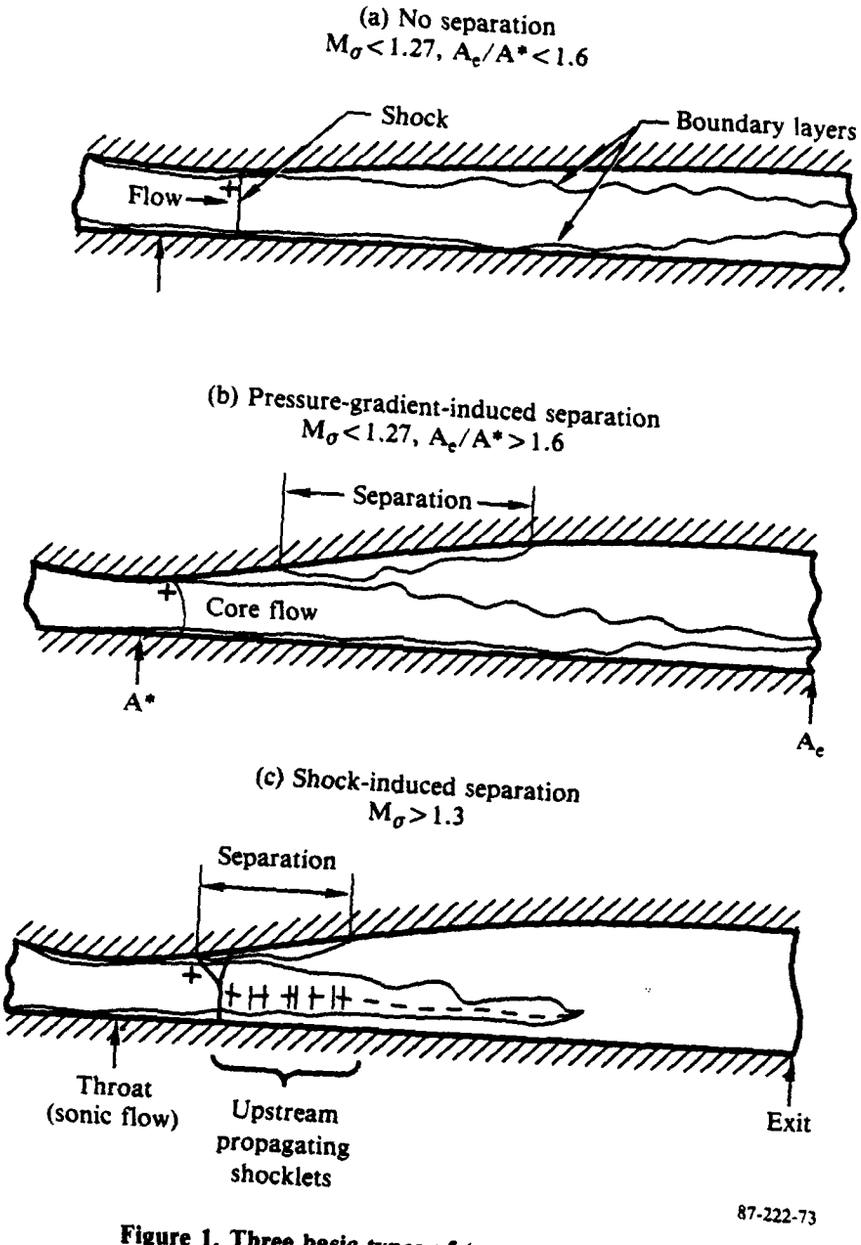

Figure 1. Three basic types of transonic diffuser flows. M_σ is Mach number at + signs.

mechanisms are responsible for the unsteadiness, as in Fig. 2, measurements yield only the combined response of all mechanisms; the contributions of the individual elementary waves cannot be singled out for separate examination.

This difficulty does not exist if a single-pulse excitation is applied. In this case, the individual waves can be separated. Thus the purpose of this contract was to devise a method for producing such excitation and use it to

examine the mechanisms responsible for the unsteadiness in a transonic diffuser flow.

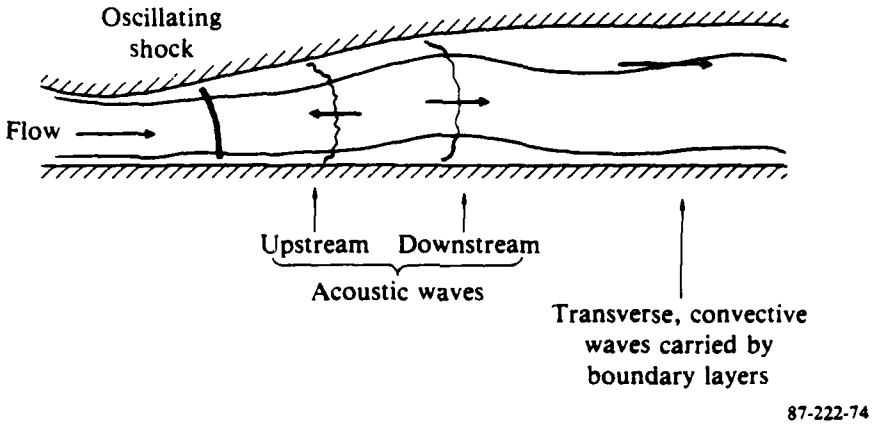

Fig. 2 Waves associated with self-excited transonic diffuser flow oscillations.

2. OBJECTIVES

The basic concept for the experimental work which is the subject of this contract is shown in Fig. 3. A means would be developed by which an abrupt pressure rise could be imposed and subsequently sustained at the downstream end of a transonic diffuser flow. The pulse would initiate an upstream-moving compression wave that, upon reaching the shock, would create both acoustic and convective reflections. The three waves would then be separable by virtue of their individual signatures on, for instance, wall-pressure measurements, as shown in Fig. 3.

The specific tasks for this contract are as follows.

Task 1 Develop a device capable of generating abrupt, ramp-type pressure pulses in a supercritical diffuser flow. The device will be compatible with an existing MDRL-provided diffuser model.

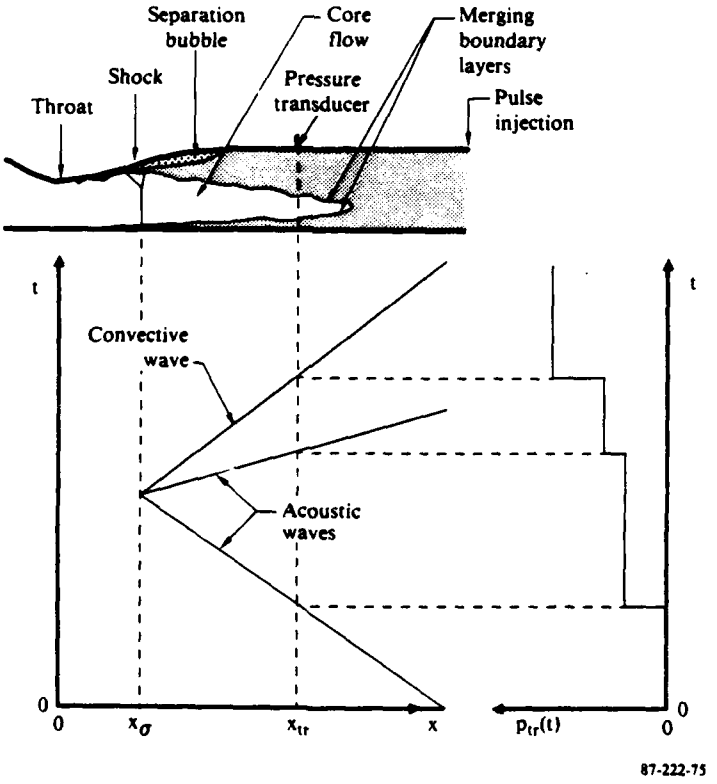

Fig. 3 Features of strong-shock diffuser flow and conceptual description of pulse propagation.

Task 2 Connect the pulse generator to the diffuser model and install in test facility. Install a traversable, fast-response, total/static-pressure-probe instrumentation system and interface to the MDRL laboratory computer. Develop the specialized control and software required. Check out all systems and conduct preliminary tests to verify correct operation of the computer and inlet model and obtain preliminary data.

Task 3 Conduct test program: acquire and reduce final data for entire shock-strength range. Make results available to other NWC-designated investigators as early as possible. Document results.

The development of the technique (Tasks 1 and 2) has been documented in the open literature (Pubs. 1, 2) and only a brief review will be given here. The purpose of this report is to provide an overview of the entire program, assemble the results of the various task phases and activities into a single publication, and document the final experimental results (Task 3).

3. EXPERIMENT

3.1 Diffuser Model and Flowfield

The diffuser model used in this study is a nominally two-dimensional, converging-diverging channel (Fig. 4). The channel has an exit-to-throat area ratio of 1.52. Side- and bottom-wall boundary layer growth is limited by three sets of forward-facing (ram) suction slots. The top-wall boundary layer is tripped 6.92 throat-heights upstream of the throat. The model side walls are fitted with schlieren-quality glass panels that allow the employment of optical diagnostic techniques.

Two reference locations are defined. The exit station at $x/h^* = 8.65$, within the constant-area section of the channel downstream of the divergent section, has been used to provide the downstream boundary condition for computational analyses intended to describe the flow. A second (pulse)

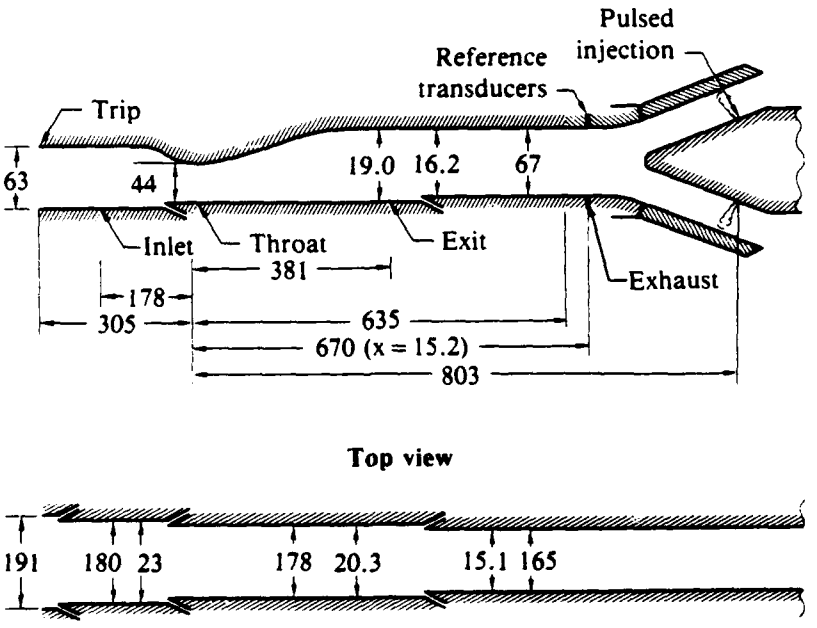

Dimensions in mm.
Vertical dimensions doubled.
Slot sizes enlarged for clarity.
Percentages denote area decrease at slots.

87-222-76

Fig. 4 Diffuser model.

reference location at $x/h^* = 15.2$ is the station at which the initial conditions of the injected pulse are determined.

Of the three types of flow shown in Fig. 1, only the top (weak-shock) and bottom (strong-shock) cases are observed in this diffuser. Spark schlieren photographs of the experimental flowfields corresponding to these two cases are displayed in Fig. 5. The weak-shock case ($M_\sigma = 1.235$) has thin boundary layers and attached, well-behaved flow. The strong-shock case ($M_\sigma = 1.353$) displays a characteristic massive separation with the top and bottom wall boundary layers merging after approximately five throat-heights.

In addition to the obvious differences between the mean flowfield properties of these two flows, there are also significant differences in their dynamic characteristics.

For the weak-shock case, the power-spectral-density (PSD) distribution of any measured quantity shows up to three distinct peaks which are associated with large-scale coherent oscillations extending throughout the entire subsonic flowfield.[14] The frequencies associated with these modes of oscillation are adequately predicted on the basis of simple linear acoustic theory.

For the strong-shock case, the PSD contains only one peak, which is not describable by acoustic theory. The conjecture has been that the mode of oscillations for this case is comprised of several elementary waves, which may

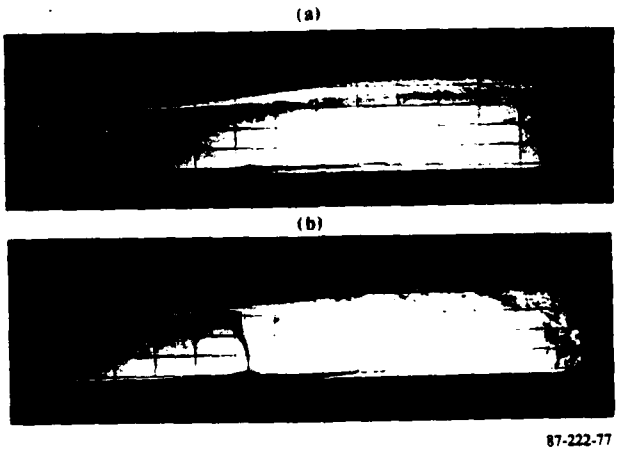

Fig. 5 Spark-Schlieren photographs of attached and separated flow. (a) $p_o/p_e = 1.225$ (weak shock), b) $p_o/p_e = 1.395$ (strong shock). Grid spacing is 24.5-mm horizontally and 12.7-mm vertically.

include upstream- and downstream-traveling acoustic waves, and a convective boundary layer disturbance.[18] The boundary conditions for the acoustic waves are an open-ended duct at the downstream end, and the shock at the upstream end. The acoustic reflection at the shock is determined by the Rankine-Hugoniot conditions, as they apply to a compression wave incident upon a normal shock. This interaction also displaces the shock upstream, which introduces a corresponding change in the boundary-layer properties. These changes are convected downstream at some significantly lower speed than the core-flow velocity. Evidence of the existence of this convective wave has been extensively documented.[17]

Additional details of the mean, self-excited, and externally excited flowfields in the diffuser are presented in Refs. 14-17.

3.2 Pulse Generator

The pulse-generating system was required to be capable of generating a ramp-type pressure disturbance, i.e., a transition to a higher pressure. The magnitude of the rise must be controllable, and must be maintained for the length of time required for the disturbance to travel upstream and for any reflections to travel downstream, as indicated in Fig. 3. The total travel time is typically on the order of 5-10 ms. The rise time must be considerably shorter; the design target was 0.1 ms. The process of perturbing the flow must be repeatable in a relatively short period of time, since several pulses will be required in ensemble-averaging the transducer signals to improve signal-to-noise ratio and to eliminate pulse-to-pulse variations.

The concept adopted for the pulse-generation system is shown in Fig. 6. The flowfield perturbation in the diffuser is generated by the abrupt injection of a mass flow into the flow path. The mass flow is injected through 16 identical nozzles located in single spanwise rows, one each on the top and bottom of the injector head. The air source for the nozzles is a shock tube, operated as a shock tunnel. This apparatus provides an appropriately fast rise time; however, the duration of the pulse is limited to the usable test time of the shock tunnel, which is governed by the shock and expansion wave propagation times in the shock tube. To lengthen the test time, a secondary, blow-down air supply system with a sliding-block-type valve is employed. The shock activates the sliding-block valves. The secondary system does not have the fast rise-time of the shock tube, but is capable of

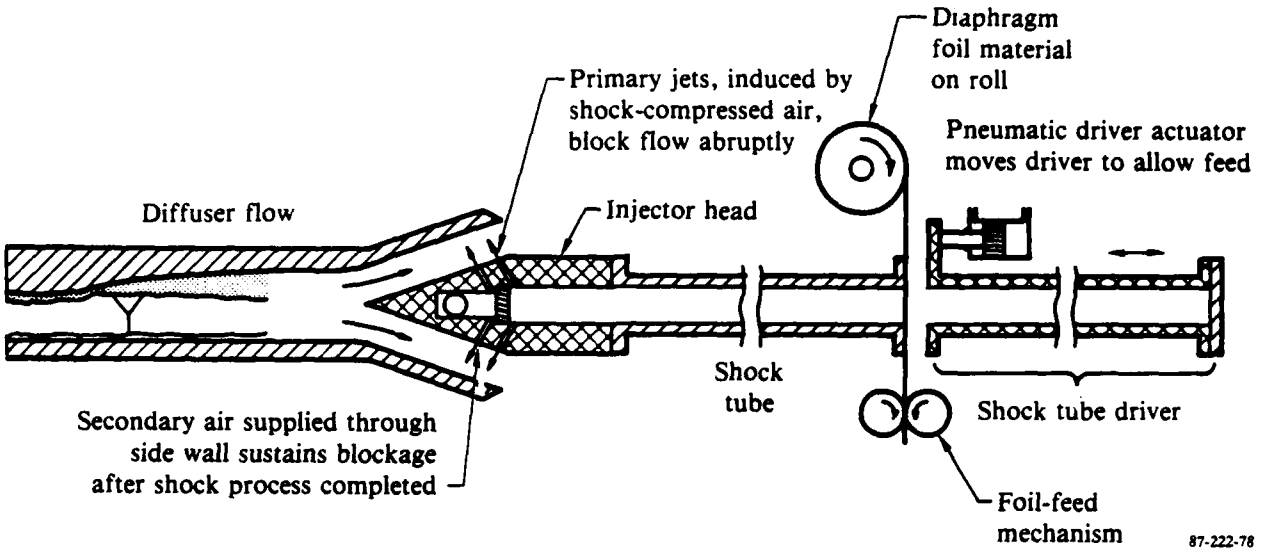

Fig. 6 Pulse generating system details.

extremely long pulse durations, depending on the secondary air source. The secondary air is injected into the diffuser flow through a second set of spanwise holes on the top and bottom of the injector head that are identical to, and just upstream of, the primary injection jets from the shock tube. The two systems working together satisfy the requirements of fast-rise-time and long-duration pulses. A more detailed description of the pulse system is provided in Pubs. 1 and 2. Figure 7 is a photograph of the pulse-injection system attached to the diffuser model.

The pressure ratio in the diffuser (ratio of stagnation to exit static pressures, p_o/p_e) is controlled by the two hinged throttle flaps, one for each passage around the pulse injector head. The flaps are also used to compensate for asymmetries in the diffuser flow. Splitting the diffuser flow halves the time required for the jet fluid to traverse the diffuser flow. However, splitting the flow can also create a problem in that the upstream travel time of the induced pulse in the top and bottom channels may be different if the two channels contain different flow velocities. Such is the case in the strong-shock flow where the diffuser flowfield is asymmetric from top to bottom. Care was taken to adjust the flaps such that the two pulses arrived at the pulse reference location ($x/h^* = 15.2$) simultaneously.

87-222-79

Fig. 7 Diffuser model and pulse generating system.

Figure 8 shows traces from transducers mounted on the top and bottom walls of the diffuser model at the pulse reference station. The rise time of approximately 75 microseconds meets the targeted value. The close agreement between top and bottom wall pressure histories indicates nearly simultaneous arrival of the pulses, i.e., a single planar wave front propagating upstream.

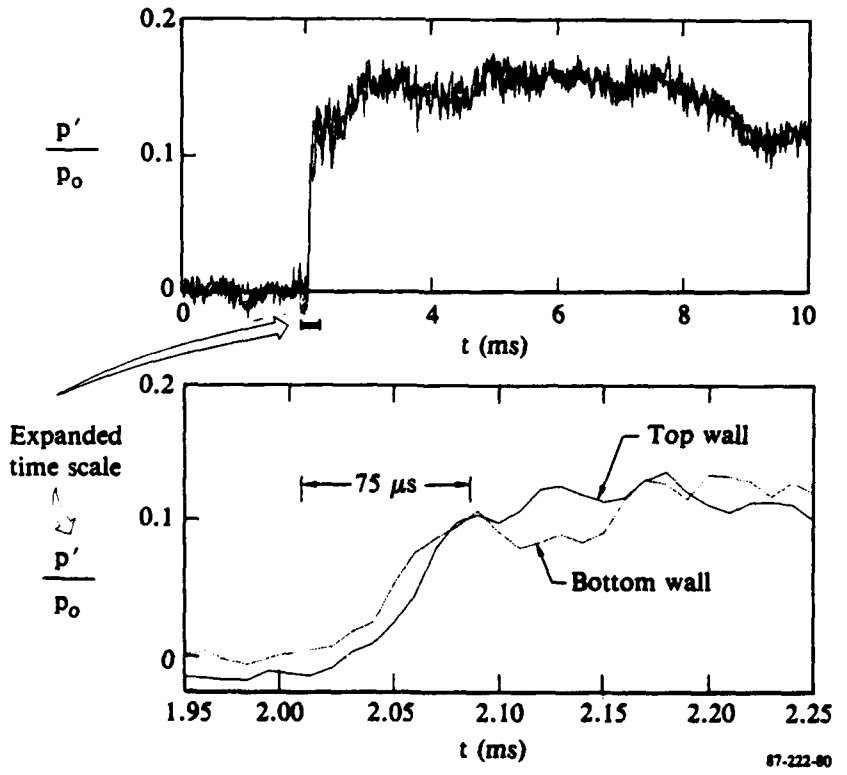

Fig. 8 Top and bottom-wall static pressure histories, $x/h_e = 15.2$

The existence of a truly planar wave front was further confirmed by introducing a third static-pressure transducer in midstream at the reference location, and verifying that its measurement of the pressure rise corresponded in time and amplitude to the wall measurements.

The operation of the pulse-generation system is entirely computer-controlled. A schematic of the various actuation controls is presented in Fig. 9. After each shot, the driver section of the shock tube is retracted and the diaphragm foil material is advanced. The sliding-block valves for the secondary air supply are reset. The driver section is closed and pressurization begins. The driver chamber pressure is monitored by the computer, and when the desired pressure is reached, a knife blade is thrust through the foil. The entire cycle takes less than 10 seconds, so a relatively short run time is required to acquire sufficient data for ensemble averaging.

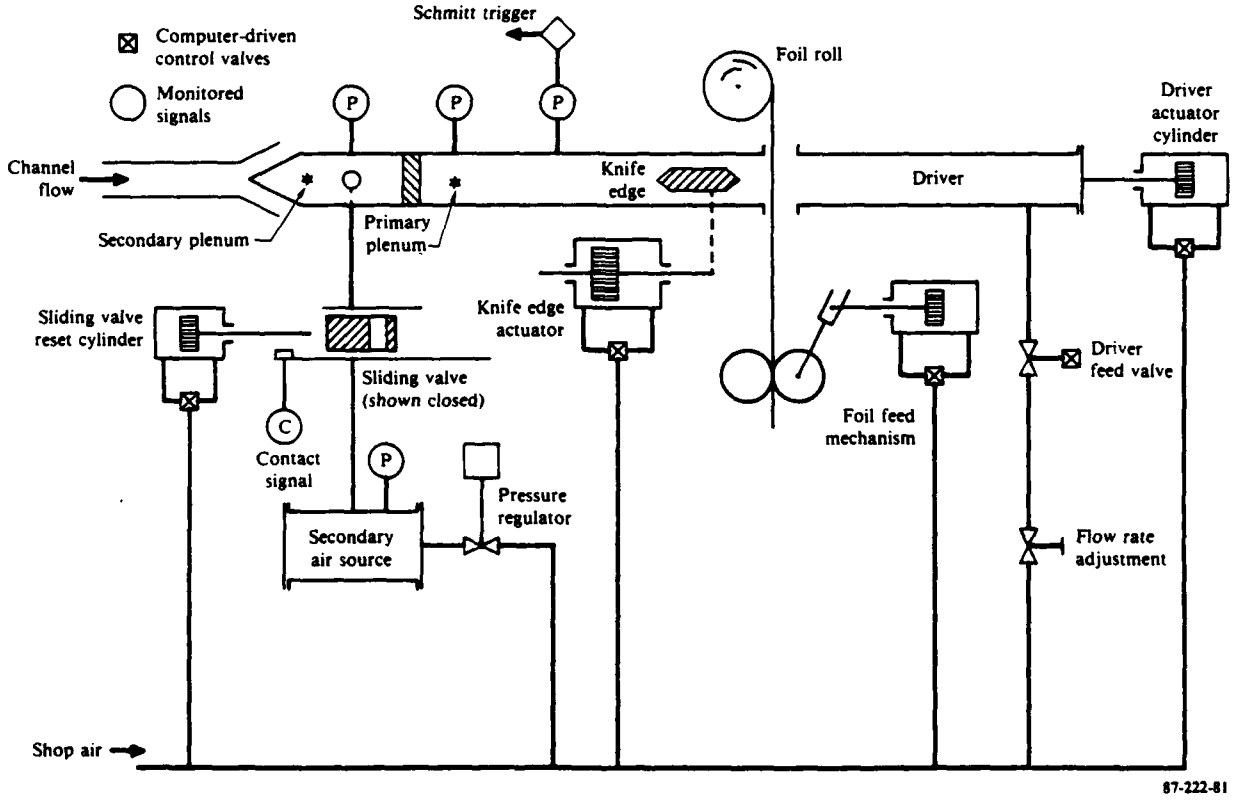

Figure 9. Details of air supply and control systems for pulse generator.

A set of typical operating conditions for the pulse-injection system is provided in Table 1. Driver pressures from 70 kPa to 350 kPa were generally used for the experiments. These pressures generated pulse strengths which varied over a 3:1 range, as measured at the pulse reference station.

Table 1. Typical Shock Tube Operating Conditions

Pressure in driver before firing	375 kPa
Pressure in tube before firing	100 kPa
Temperatures in tube and driver	300 K
Shock speed	460 m/s
Pressure of doubly-shocked gas	333 kPa
Temperature of doubly-shocked gas	428 K
Jet Mach number	1.43
Jet speed	500 m/s
Duration of steady jet flow	5.2 ms
Time for jets to traverse a channel branch (set to 2.0-cm height)	40 μs

87-222-71

3.3 Instrumentation and Data Acquisition

The diffuser operating condition was routinely monitored and recorded, including measurements of the diffuser supply plenum static pressure and temperature (diffuser total pressure and total temperature), the diffuser pressure ratio, and atmospheric pressure. In addition, the burst pressure of the shock tube driver was recorded for each shot in order to determine the amount of shot-to-shot variation. With the computer-triggered diaphragm burst procedure, this variation was on the order of 3.5 kPa (rms).

The top wall of the diffuser model is fitted with seven flush-mounted, fast-response pressure transducers, distributed from the vicinity of the shock to just upstream of the injector head. The pulse reference signals are used to determine the pulse strength, which is used in the data reduction to normalize the rest of the wall pressures. In addition, a fast-response transducer was located in the driven side of the shock tube near the injector head to trigger the high-speed data acquisition system.

A traversable twin total/static "core" probe (similar to that described in Ref. 16) fitted with fast-response transducers was used to map the unsteady

pressure field in the core flow. The probe could be moved vertically along the full height of the channel, and in the streamwise direction from the shock to just upstream of the exit station.

Optical data were also acquired. High-speed schlieren movies (10,000 frames/s) were made to document the shock response to the pulse impingement. The movies became a valuable diagnostic tool, especially for the weak-shock case in which it was found that the same pulse strength used for the strong-shock case would drive the weak shock completely through the throat, i.e., the pressure rise imposed at the downstream end of the diffuser generated a pressure ratio corresponding to fully subsonic flow in the diffuser (subcritical operation). Hence, a weaker pulse was used for the weak-shock flow to maintain fully supercritical operation. In addition, a real-time shock-position-indicating system[24, 25] was used to measure the time history of the shock location, corresponding to the time histories of the wall and core pressures.

All unsteady data were digitized at 50 kHz/channel. This provided 20-microsecond resolution which was deemed sufficient. Trials with digitization rates up to 100 kHz/channel were made; no significant difference appeared in the data. Ensemble averages were made over 25 shots for all data. Trials were made for ensemble averaging of 10 to 50 shots. It was found that for more than 25 shots, no significant changes or smoothing appeared in the data.

3.4 Test Conditions

The shock Mach-number range examined was $1.18 < M_\sigma < 1.38$, with the transition from weak-shock to strong-shock flow occurring at about $M_\sigma = 1.273$. This Mach-number range corresponds to a pressure-ratio range of $1.21 < p_o/p_e < 1.41$. Wall-pressure measurements were taken at 10 pressure ratios covering this entire range. Two shock Mach numbers ($M_\sigma = 1.251$ and $M_\sigma = 1.378$) were selected for detailed examination. For these two cases, a study was made of the effect of pulse strength on the pulse propagation characteristics, and core-probe surveys were taken.

For the strong-shock data, the driver pressure was set at 275 kPa. This created a pulse whose strength was 6.3% of the local time-mean static pressure as measured at the injector head reference station. For the weak-shock core-probe data, the driver pressure was 137 kPa, creating a pulse strength of 3.0%.

The initial runs revealed that the primary pulse provided by the shock tube system had a sufficiently long duration for the upstream and downstream waves to complete their travel. The secondary air-injection system thus was not required and its use was discontinued.

4. RESULTS

4.1 Wall-Pressure Measurements

A sample set of time histories of the top-wall transducers is shown in Fig. 10 for a weak- (M_σ = 1.251) and strong-shock flow (M_σ = 1.378). Passage of the upstream-traveling acoustic wave can clearly be seen as the sharp rise in the signal. The rise occurs progressively later at each successive upstream measurement station. The pulse is initially quite steep, but broadens as it approaches the shock.

In all of the weak-shock cases, only the upstream-traveling acoustic wave appears; there is no observed reflection of any sort. This is consistent with linear acoustic theory, which predicts negligible acoustic reflection for weak shocks.[26] In the strong-shock case, however, the reflection is strong and can be seen clearly as a secondary rise in the pressure signals (arrows), which occurs at later times at the more downstream stations.

From transducer-signal time histories such as those presented in Fig. 10, x-t diagrams can be generated from which the wave propagation speeds can be determined. Figure 11 contains an x-t diagram for both the pulse propagation (Fig. 11b) and the response of the shock to the impingement of the acoustic pulse (Fig. 11a).

Figure 11b contains the pulse-propagation information for a weak shock (M_σ = 1.251), a strong shock (M_σ = 1.378), and a case where the shock is just strong enough to cause a shock-induced separation (M_σ = 1.292). It was found that the speed of all waves was nearly constant over the length of their travel; the x-t diagrams are essentially straight lines. The reflected waves in the strong-shock cases are clearly convective, as indicated by the relatively slow speed of 95 m/s (an acoustic wave would travel 4-5 times as fast). No evidence of a reflected acoustic wave was observed for any of the flows.

If the strong-shock case acoustic- and convective-wave trajectories in Fig. 11 are extrapolated upstream, then the locations where they cross are nearly midway between their respective undisturbed and final shock locations. That the convective wave for the M_σ = 1.292 case is delayed somewhat from that of the M_σ = 1.378 case results from the fact that the undisturbed shock location for the weaker of the two shocks is farther upstream and the acoustic

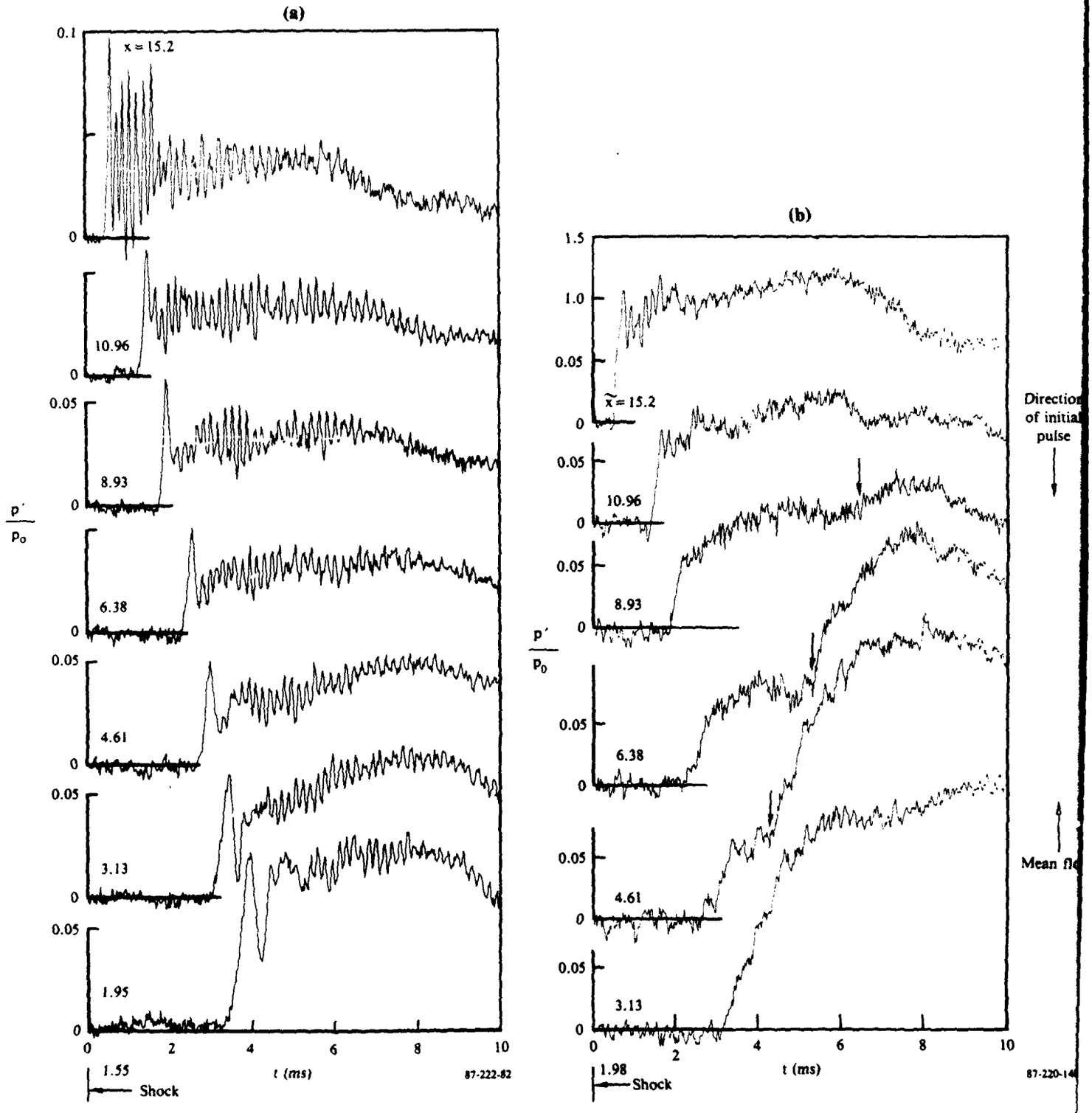

Fig. 10 Time histories of top-wall static pressure: (a) $M_\sigma = 1.251$; (b) $M_\sigma = 1.378$. Annotation denotes streamwise transducer location.

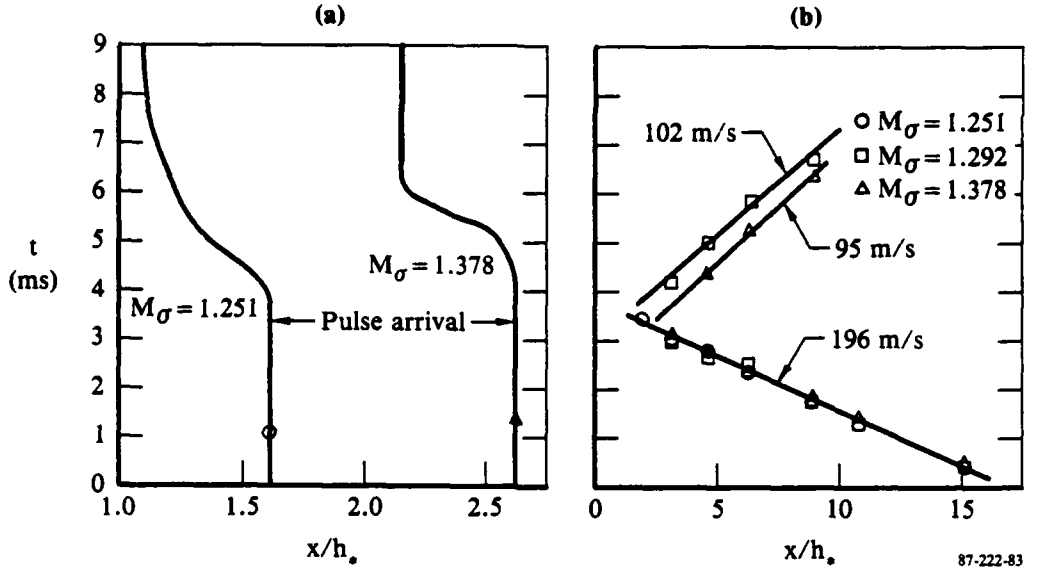

Fig. 11 x-t diagram of weak and strong-shock flow response to pulse: (a) instantaneous shock location (horizontal scale expanded); (b) pulse propagation measured along top wall.

wave must travel that much farther before encountering the shock. This was found to be the case for all strong-shock flows examined. There is no measurable time delay between the impingement of the acoustic wave and the generation of the convective wave.

Table 2 contains a summary of the wave propagation speeds for all the flows examined. In spite of the complex, decelerating, sometimes separated flowfields in each of these cases, the propagation speeds seem remarkably independent of pressure-ratio effects. The upstream speed (w_-) is consistently around 200 m/s, and the downstream speed (w_+) is approximately half that. The observed w_- values are unexpectedly high, especially near the shock where the core-flow velocity is the highest. This phenomenon is examined in more detail in Section 5.2.

The shock response to the impinging acoustic pulse (Fig. 11a) shows different characteristics for the weak- and strong-shock cases. For the weak shock, the shock responds almost instantaneously as the acoustic pulse impacts, but the time required for the shock to assume its new equilibrium location corresponding to the lower pressure ratio created by the pulse is relatively long. On the other hand, for the strong shock, there is a delay of 1 - 1.5 ms before the shock responds to the acoustic wave, by which time the

Table 2. Wave Propagation Speeds

	M_σ	p_0/p_e	w_- (m/s)	w_+ (m/s)
Strong Shock:				
	1.378	1.410	199	90
	1.339	1.383	200	90
	1.320	1.359	192	100
	1.309	1.335	200	96
	1.292	1.309	199	102
	1.276	1.280	202	117
Weak Shock:				
	1.270	1.258	205	—
	1.251	1.232	205	—
	1.177	1.207	202	—

87-222-72

reflected convective wave has traveled nearly five throat-heights downstream. However, once the shock does respond, it assumes its new equilibrium location quite quickly.

A study was also made of the effect of pulse strength variation for the cases of Fig. 10. The initial pulse strength, defined as the ratio of the pressure-rise magnitude at the pulse reference station to the mean pressure at the same location, was varied over a more than 3:1 range. The results are shown in Fig. 12. Normalizing the pulses measured along the length of the model (p'_x) with the pulse reference station strength ($p'_{15.2}$) produces a good correlation of the data for both cases.

For the weak-shock case (Fig. 12a), the pulse is somewhat attenuated as it travels upstream, but rises sharply as the shock is approached. Similar trends were also found when a periodic excitation was applied to the downstream end of the same diffuser model (Figs. 9-11 of Ref. 16). This similarity between the pulsed and periodic excitation is not surprising since for weak-shock flows only the upstream-traveling acoustic wave is present, whether the perturbation is pulsed or periodic.

For the strong-shock case, the upstream wave is slightly more attenuated than for the weak shock. The reflected convective-wave amplitude is large initially, but strongly damped, diminishing to zero at approximately $x/h^* = 11$. This location is near several significant mean-flow features. The core flow terminates at $x/h^* = 8.4$, and the separation bubble terminates at $x/h^* = 6.1$. Neither of these two features exists in the weak-shock flow, which

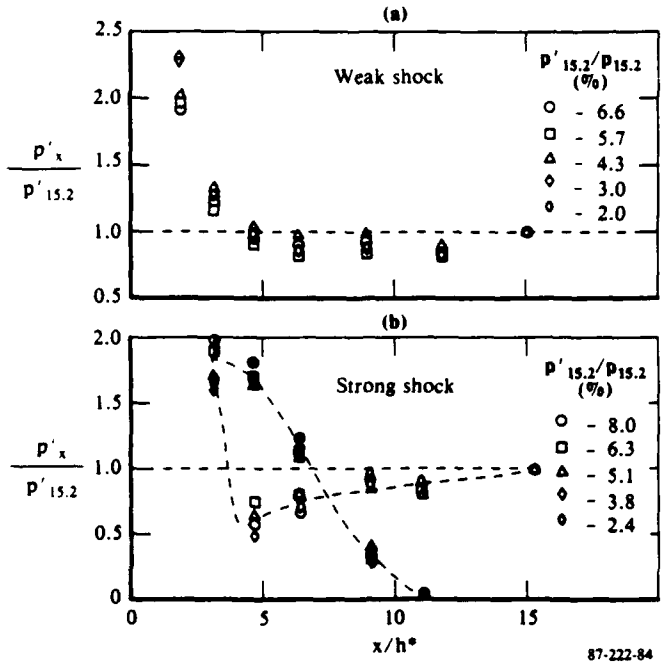

Fig. 12 Normalized pulse strength distributions: (a) $M_\sigma = 1.252$; (b) $M_\sigma = 1.378$. Open symbols: upstream-moving acoustic waves; full symbols: downstream-moving convective waves: half-full symbols: contributions from both waves present.

suggests that a thick-boundary-layer/core-flow interface and a shock-induced separation may both be related to the existence of the convective wave. In addition, from the shock to approximately x/h* = 11, the velocity profiles display inflection points in the top-wall boundary layer. This particular feature, for a free shear layer between streams of infinite extent, is known to ensure the growth of disturbances over a finite frequency range. In the present situation (wall proximity, decelerating flow, and increasing transverse spatial scale) the disturbance does not grow, but the damping is moderate enough to allow observation of the disturbance.

4.2 Core-Flow Pressure Measurements

Both total- and static-pressure measurements were made throughout the flow from just downstream of the shock to just upstream of the exit station in both the weak- and strong-shock flowfields. The total-pressure measurements are difficult to interpret alone since they are composed of fluctuations in both

static pressure and velocity. Since detailed analysis is beyond the scope of this contract, only the static-pressure data will be discussed.

For the weak-shock flow, the core-probe static-pressure signals were similar to the wall-pressure signals. The core-probe signals showed only a single abrupt rise corresponding to the upstream-traveling acoustic wave. Data from the survey have been assembled to display the propagation of the wave front. The wave front was said to have arrived when the signal significantly exceeded the pre-pulse noise level (about 1 kPa). Figure 13 shows the wave front location at every 0.1 ms. The wave front remains essentially vertical throughout its travel, indicating that the pulse is planar, despite the nonuniform velocity profile.[15] The wave speed as determined from the core-probe data is the same as that determined from the wall data.

The strong-shock core-probe data do not provide as simple a picture as the weak-shock data. Figure 14 shows the core-probe static-pressure signals at $x/h^* = 4.0$ at selected locations spanning the height of the channel. Near the top wall the core-probe data closely resemble the wall data; however, additional ripples appear in the signal, becoming more sharply defined as the bottom wall is approached. The ripples display a well-defined pattern in streamwise variation as well. Figure 15 shows core-probe pressure traces for a streamwise survey at $y/h^* = 0.3$. As the shock is approached, the number of peaks which appear increases from one at the downstream end of the surveyed

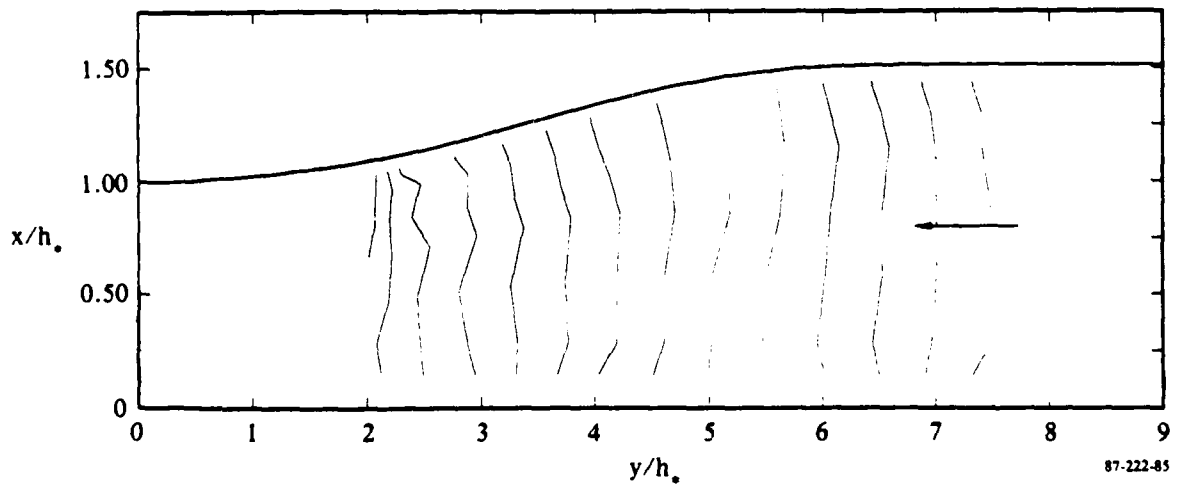

Fig. 13 Weak-shock pulse wavefront propagation. Contours at 0.1 ms intervals.

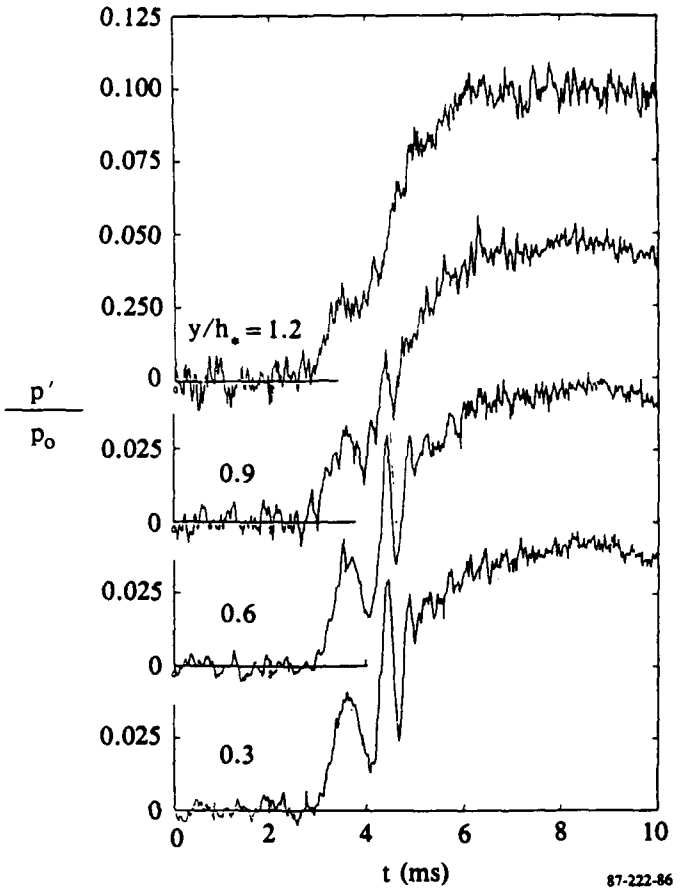

Fig. 14 Core static pressure measurements, vertical scan at $x/h_* = 4.0$.

region to three near the shock. The spacing between the peaks changes as well, indicating that the ripples are dispersive.

An attempt was made to determine the origin of the ripples. Probe interference or mechanical vibration effects were investigated and ruled out as the cause. An x-t diagram (Fig. 16a) was constructed containing the initial pulse arrival (determined as for the weak-shock case described above) and the first and second peaks, along with the convective wave. A least-squares fit was made to the data. The speed associated with the pulse arrival (203 m/s) is essentially the same as that for the pulse as measured on the top wall, while the speeds associated with the first and second peaks are 135 m/s and 93 m/s, respectively. Throughout the range where a third peak could be clearly discerned, its speed was measured to be 79 m/s.

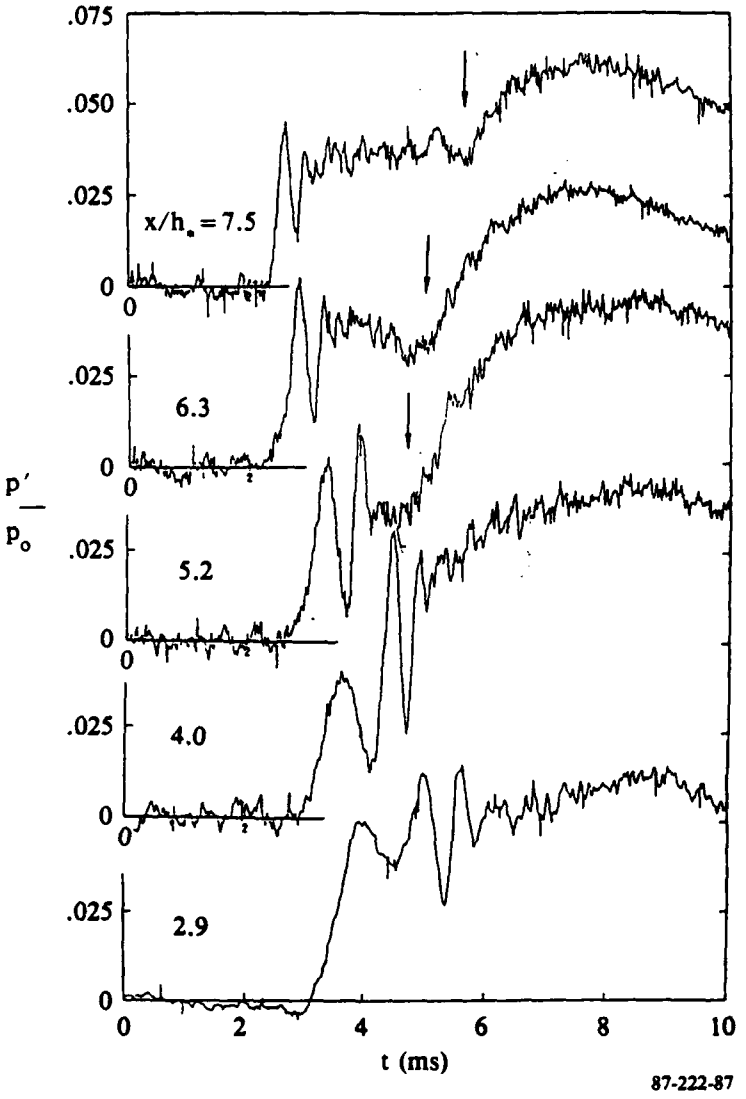

Fig. 15 Core static pressure disturbance propagation, horizontal scan at $y/h_* = 0.3$.

A striking feature of the peak trajectories is that they all seem to converge at a single point, approximately x/h* = 9.61. Figure 16b shows various features of the flowfield and model geometry. A suction slot is located at x/h* = 9.80, quite close to the intersection of the trajectories. The possibility that the suction slot and its associated plenum were acting as a Helmholtz resonator was tested and ruled out, as was the possibility that the ripples originated downstream at the injector head and the convergence of the trajectories at the slot is just a coincidence. The final conclusion is that the abrupt 12.7% area change at the bottom slot triggers the ripples;

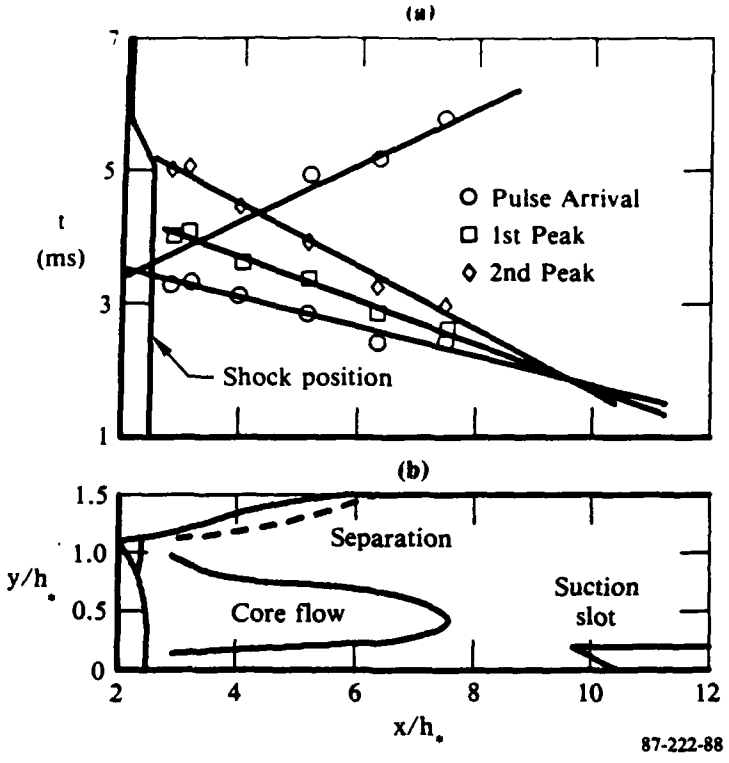

Fig. 16 Tracing origin of ripples: (a) x-t diagram of propagation; (b) model and flow features.

their prominence near the bottom wall is probably related to the fact that the suction slots exist only on the bottom and side walls, not on the top wall.

The upstream-moving compression wave, as it exists for $x/h^* > 9.80$, is the intended perturbation. The passage of the pulse through the abrupt area-change at the slot constitutes an additional perturbation modifying the pre-existing, intended perturbation. This two-stage triggering process is complex, as is the resulting wave-front structure. The evolution of the composite perturbation as evidenced by the ripples on the pressure signals is reminiscent of nonlinear gravity waves on liquid surfaces.

The mechanism for triggering the ripples is model-specific, but their positive growth rate suggests that they might occur in other situations as a result of other triggering mechanisms. The nature of the ripples is not understood, but further investigation of this phenomenon is beyond the scope of this contract.

The ripples obscure the pressure signature of the convective wave over a significant portion of the channel. Figure 16a is derived from data taken at

$y/h^* = 0.5$. In these data the convective wave cannot be observed until it is nearly four throat-heights downstream of the shock. Farther upstream, the convective wave is overlapped by the oscillations. As seen in Fig. 14, the anomalous peaks decrease in amplitude toward the top wall, but the actual arrival of the convective wave cannot be determined with confidence until very near the top wall. However, at the measurement stations nearest the top wall, the wave speeds measured by the core probe correspond closely to those obtained from the wall-pressure measurements.

5. RELATED ANALYSIS

Inspired by the experimental results obtained through this contract work, we performed several related studies under funding by the McDonnell Douglas Independent Research and Development program. These studies extended the data analysis beyond the scope of the contract, and addressed some apparently anomalous behavior in the results. These studies are briefly described below.

5.1 Resultant Wave Reconstruction

Using the amplitude and phase information from the experimental data obtained under this contract, an attempt was made to reconstruct, from the elementary waves, the oscillations found in the strong-shock case where the flow was periodically excited. (The weak-shock case is trivial, since only one wave is present.) Experimental data from Ref. 16, where the flow was excited at 100, 200, and 300 Hz, are used for comparison. The success of such a reconstruction would prove that the elementary wave properties determined experimentally from the pulse tests form a valid basis for modeling a variety of unsteady flows.

The reconstruction was accomplished by forming two, counterpropagating, simple, single-frequency waves having the streamwise amplitude distributions and speeds measured for the elementary waves from this pulsed experiment. The individual wave numbers were derived from the wave speed and frequency. These two waves were then simply added together. Special considerations involved in determining the relative amplitudes and phases of the component waves are discussed below.

Separation of amplitude contributions from the upstream- and downstream-traveling waves on the basis of the wall-pressure measurements alone is not possible near the shock. The time delay between the two waves as they pass over the transducer is negligible and the signal shows only a single rise (Fig. 10b, $x/h^* = 3.13$). The uncertainty of the relative contributions from the two waves at this location is emphasized by the half-filled symbols in Fig. 12b. The convective-to-acoustic amplitude ratio at the shock, based on the data trends farther downstream, was estimated to be 3:2. (Further analysis of the core-probe data is required to refine this estimate.)

The phase relation between the two waves was initially determined by considering the x-t diagram in Fig. 11b. The negligible time delay between the impingement of the acoustic wave and generation of the convective wave indicates that there is no phase shift between the upstream- and downstream-traveling waves at the shock. This observation, coupled with the estimated amplitude relation discussed above, yields a reflection coefficient of 1.5; and since the pulse reflection appears with no time delay and has the same sense as the incident wave (pressure rise), the reflection coefficient for a harmonic wave based on the pulse response would be a real, positive number.

It is not certain to what degree the phase relations implied in the pulse experiment can be extended to the case of harmonic waves; the spectral contents of the two waves are completely different. Analysis of normal shock response to harmonic acoustic waves[26] predicts a frequency-dependent phase shift at the shock. The considerable delay between the arrival of the acoustic wave and the eventual recoil of the shock (Fig. 11) also implies that some additional phase shift may occur in the harmonic case. To optimize the agreement between the reconstruction and the experimental data, an additional delay of 0.5 ms between the upstream- and downstream-traveling waves at the shock was incorporated in the reconstruction for all cases.

The results of the wave reconstructions are shown in Fig. 17. The experimental phase data were referenced to the angular position of the mechanical excitation device; hence, the relative phase relation between the data and the reconstruction is unknown since no equivalent reference exists for the pulse experiment. The reconstructed phase data were arbitrarily shifted to agree with the experimental data near the shock, with the same shift applied to the rest of the downstream data. In addition, it has been the practice with this model to normalize amplitude data with the amplitude at the exit station. Figure 17 follows this practice; the experimental amplitudes and the reconstruction have been normalized with their respective values at $x/h^* = 8.65$.

The agreement of the phases between the experimental data and the reconstruction is excellent for the 100-Hz and 200-Hz cases. The agreement for the 300-Hz case is less striking, although the major trends in the reconstruction still follow those of the experimental data. The major discrepancy is the failure of the reconstruction to capture the sharp phase-shift at the node at $x/h^* = 3.8$. However, a sharp phase-shift can only occur

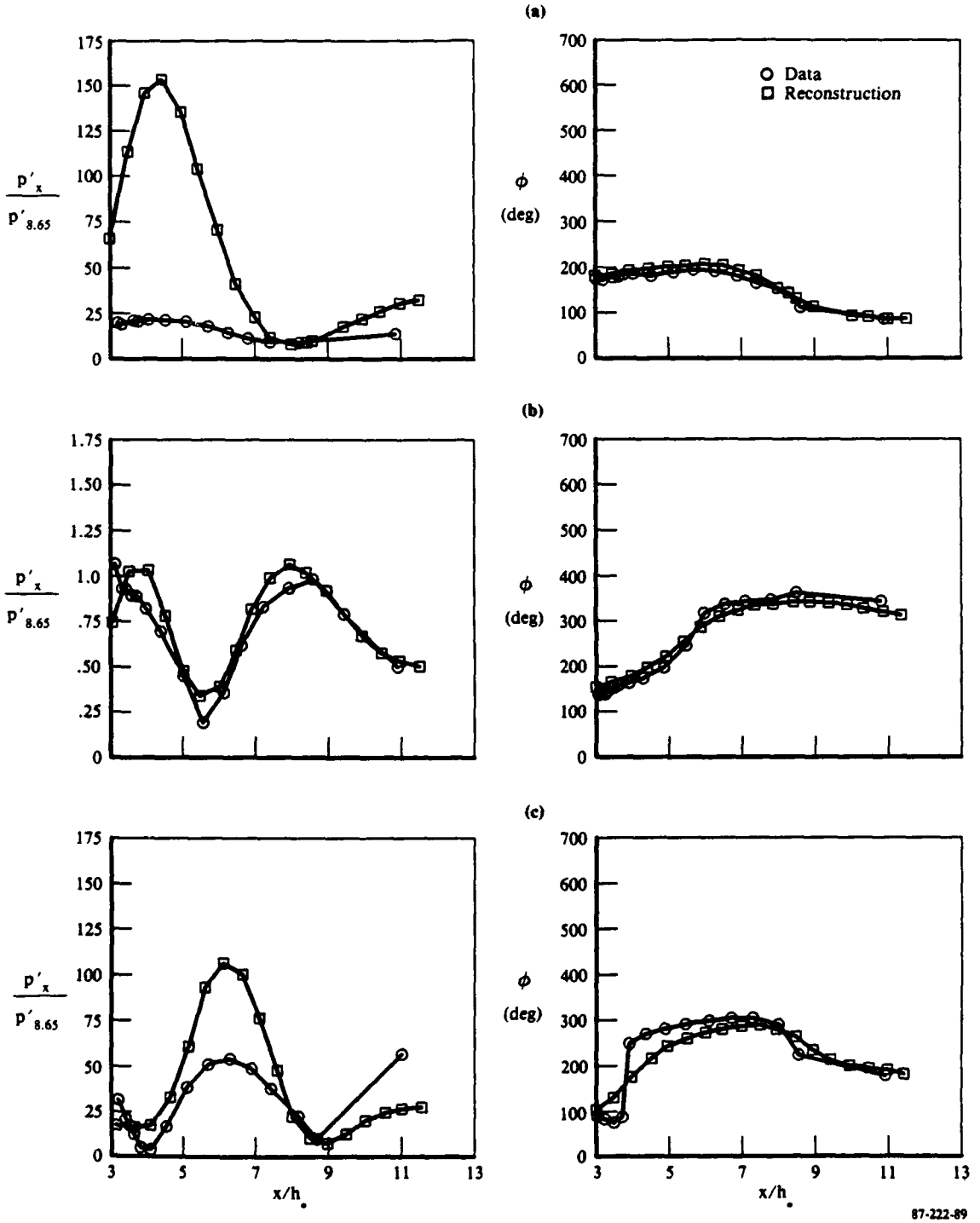

Fig. 17 Comparison of experimentally determined amplitudes and phases for periodic excitation with reconstruction from elementary waves, strong-shock flow: (a) f = 100 Hz; (b) f = 200 Hz; (c) f = 300 Hz.

if there is exact cancellation between the two counter-propagating waves, which requires that the two waves have identical amplitudes at that point. Given the uncertainty in estimating the relative wave amplitudes near the shock, it is not surprising that this particular feature is not well reproduced.

A heretofore puzzling feature of the experimentally determined periodic phase distributions is the evidence of an upstream propagating wave (decreasing phase with increasing distance) past the end of the core flow ($x/h^* > 8$) present in all three cases. It was expected that the externally imposed periodic excitation would generate a simple standing-wave-like amplitude envelope (nodes and antinodes) superimposed over a traveling wave.[18] However, given the results shown in Fig. 12b, the reason for the observed behavior becomes evident. Downstream of the core flow, the downstream-traveling convective wave has completely died out. The upstream-traveling acoustic wave is the only one present and hence, the only influence observed.

The amplitude distributions for the experimental data and the reconstructions also show qualitative agreement; the trends of maxima and minima are faithfully represented; however, there is considerable difference in the relative magnitudes. For the 100-Hz case, the reconstructed amplitudes are large everywhere. Near the shock, the reconstructed peak is nearly an order of magnitude larger than the data. The 300-Hz case shows only about a factor of two difference between the data and the reconstruction. At $x/h^* = 6$, the reconstructed peak is larger, but the apparent approach to a peak just past $x/h^* = 11$ shows the data to be larger. The 200-Hz case shows excellent agreement. (It might be noted that 200 Hz is near the self-excited oscillation frequency for this diffuser, 217 Hz.)

Finally, with regard to the self-excited oscillations, Ref. 14 found that for the strong-shock flow the self-excited frequencies could not be described by simple acoustic theory. The frequencies did not scale with the length of the subsonic flowfield, but rather with the core-flow length. Using the wave speeds measured in this pulsed experiment, predictions were made of frequencies by calculating the round-trip travel time based on the measured core-flow length[14]. This procedure implies that the convective wave generates an upstream-traveling acoustic wave at the downstream end of the core flow by some (as yet unknown) mechanism. The acoustic wave, in turn, generates another convective wave when it reaches the shock. The results are shown in

Fig. 18. The agreement between the self-excited data and the prediction is quite good, strongly suggesting that the mechanism responsible for the self-excited oscillations consists of a cycle involving the convective and acoustic waves.

This analysis of the pulsed data shows that the measured oscillations occurring in both the self-excited and externally excited strong-shock diffuser flow result from the interaction of elementary waves, a fact which until now has only been conjecture. It also indicates that these elementary waves are the upstream-traveling acoustic wave and a downstream-traveling convective wave observed in the pulsed-flow measurements.

5.2 Pulse Propagation in Nonuniform Channel Flows

An anomalous finding described in section 4.1 is that the speed of the upstream-propagating acoustic wave is considerably faster, especially near the shock, than would be predicted on the basis of core-flow properties. Since knowledge of the wave speed is necessary to calculate the self-excited frequencies of a diffuser, a simple analytical method for predicting the wave speed was developed for nonuniform channel flows.

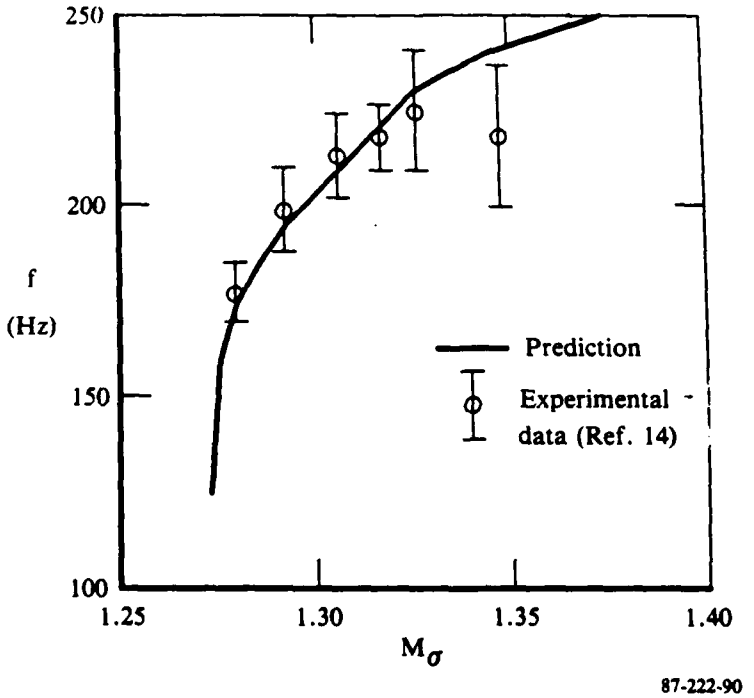

Fig. 18 Comparison of self-excited frequency prediction based on elementary wave properties obtained from experimental data.

Viscous effects enter into the analysis only in that they are responsible for the nonuniformity of the velocity and density profiles; they are otherwise neglected. The pressure is assumed constant normal to the flow, and the shape of the cross section and the flow property profiles may be specified arbitrarily.

Weak compression waves are treated by requiring the conservation of mass, momentum, and energy, all of which are expressed as appropriate integrals over the entry and exit surfaces of a control volume fixed to the wave. The integrals are expressed in terms of shape factors and mean-flow properties. The major assumption made is that the shapes of the density and velocity profiles (and hence the shape factors) are the same on both faces of the control volume; only the magnitude of these quantities is changed by the passage of the wave. Since the shape factors are known from the specification of the initial profiles, the number of unknown properties behind the wave is reduced to three, and can thus be computed from the three available equations.

Through the above formalism, the wave speed can be determined by use of shape factors computed from the velocity profiles as measured relative to the wave. Since the wave speed is not known initially, the wave speed and the shape factors appropriate for the coordinate system moving with the wave are determined simultaneously.

Results of applying the above technique to several numerical test cases show good agreement with numerical predictions.[27] Figure 19 shows the dependence of wave speed on boundary-layer thickness for a simple profile constructed of a constant-speed core flow and a parabolic boundary-layer.

This technique was also applied to the weak- and strong-shock flowfields examined in this study. Figure 20 shows a comparison of the experimental data, the wave speed predicted through application of 1-D gas dynamics using the core flow conditions, and the prediction based on the present theory. Although a minor discrepancy still remains near the shock, the present theory predicts the wave speed remarkably well. The comparison indicates that although the theory was derived for constant-area channels, it is adequate for cases in which the cross-sectional area varies slowly, provided that the calculation is based on local flow profiles. Details of this theory are presented in Ref. 28.

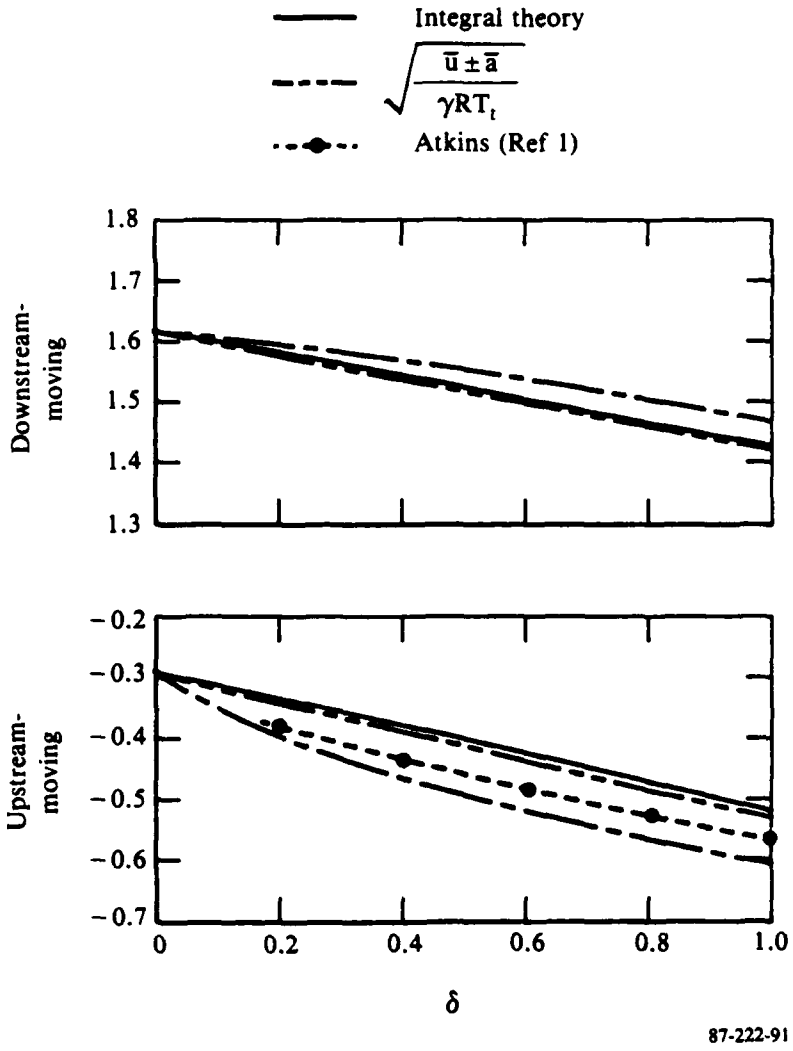

Fig. 19 Dependence of normalized wave speed on boundary layer thickness. Core flow Mach number is 0.7. (From Ref. 28).

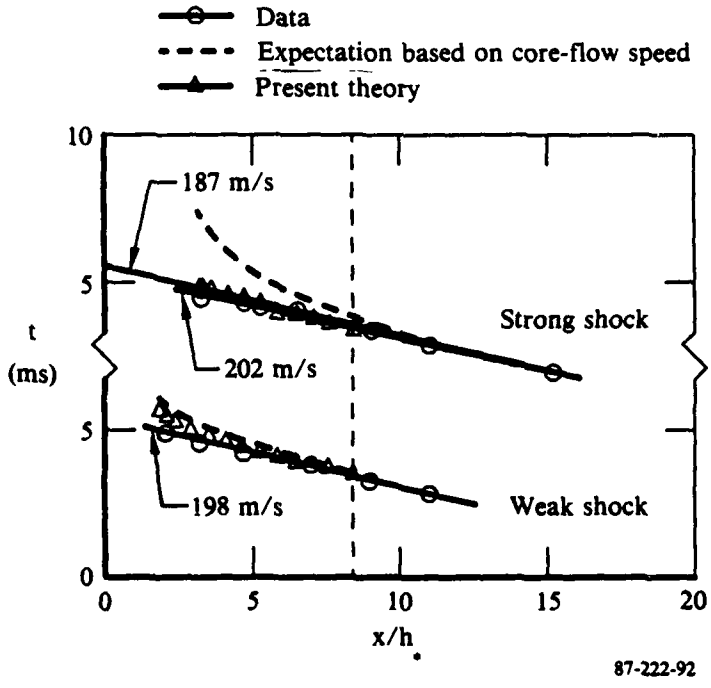

Fig. 20 Trajectory of upstream-moving wave.

6. SUMMARY

The significant accomplishments and results of this program are the following.

* A fast-rise-time pulse generator was designed and constructed, and operated according to expectations.

* When used with a transonic diffuser, the pulse generation technique was capable of separating the elementary waves for individual investigation.

* Of the three elementary waves conjectured to exist in transonic diffuser flows, only two (upstream-traveling acoustic and downstream-traveling convective waves) were found to exist in the strong-shock flow, while only the upstream-traveling acoustic wave was found in the weak-shock flow.

* The amplitude distributions and phase relations of the elementary waves were determined.

* The pulse reflection coefficient at the shock for the weak-shock case was found to be zero, while for the strong-shock case it was estimated to be 1.5.

* The convective wave was strongly damped and existed only in those regions where the velocity profile possessed an inflection point.

* From the elementary wave information determined in this program, features of the resultant wave patterns for periodically excited strong-shock flow could be reconstructed with reasonable agreement, and the frequencies for the self-excited strong-shock flow could be predicted.

* Core-flow measurements for the weak-shock case showed a planar (one-dimensional) acoustic wavefront structure at all locations in the flow, with wave speeds corresponding closely to those obtained from wall-pressure measurements.

* Core-flow measurements for the strong-shock case revealed a family of rapidly growing ripples superimposed on the original pulse.

7. PRESENTATIONS AND PUBLICATIONS

(based completely or in part on work done under this contract)

1. Sajben, M. and Kroutil, J. C., "Concept and Technique for Probing Channel Flows with Abrupt Perturbations", AIAA Paper No. 86-0311, January 1986.
2. A revised version of the above paper with the same title has been accepted by the Journal of Propulsion and Power.
3. Sajben, M., Bogar, T. J., and Atkins, H. L., "Propagation of Weak Shocks in Nonuniform Channel flows", US/French Combustion Instability Workshop, Naval Weapons Center, China Lake, CA, April 1986.
4. Bogar, T. J. and Sajben, M., "Response of Transonic Diffuser Flows to Abrupt Increases of Back Pressure: Wall Pressure Measurements, 23rd JANNAF Combustion Meeting, October 1986, CPIA Pub. 457.
5. Because of the limited distribution of JANNAF Proceedings, the above paper will also be presented at the AIAA 19th Fluid Dynamics, Plasma Dynamics, and Lasers Conference, June 1987.

8. REFERENCES

1. Martin, A. W., "Propulsion System Flow Stability Program (Dynamic) - Part 1," AFAPL-TR-68-142, 1968.
2. Ferri, A. and Nucci, L. M., "The Origin of Aerodynamic Instability of Supersonic Inlets at Supercritical Conditions," NACA-RM-L50K30, Jan. 1951.
3. Fisher, S. A., Meale, M. C., and Brooks, A. J., "On the Sub-Critical Stability of Variable Ramp Intakes at Mach Numbers Around 2," National Gas Turbine Establishment, England, Rept. ARC-R/M-3711, Feb. 1970.
4. Clark, W. H., "Static and Dynamic Performance Investigations of Side Dump Ramjet Combustors: Test Summary," Naval Weapons Center, China Lake, CA, NWC TP 6209, Dec. 1980.
5. Clark, W. H., "Geometric Scale Effects on Combustion Instabilities in a Side Dump Liquid Fuel Ramjet," CPIA Pub. 366, Vol. I, 1982, pp. 595-604.
6. Schadow, K. C., Crump, J. E., and Blomshield, F. S., "Combustion Instability in a Research Dump Combustor: Inlet Shock Oscillations," CPIA Pub. 347, Vol. III, 1981, pp. 341-356.
7. Crump, J. E., Schadow, K. C., Blomshield, F. S., and Bicker, C. J., "Combustion Instability in a Research Dump Combustor: Pressure Oscillations," CPIA Pub. 347, Vol. III, 1981, pp. 357-370.
8. Rogers, T., "Ramjet Inlet/Combustor Pulsation Analysis," Naval Weapons Center, China Lake, CA, NWC TP 6053, Jan. 1980.
9. Rogers, T., "Ramjet Inlet/Combustor Pulsation Analysis," Naval Weapons Center, China Lake, CA, NWC TP 6155, Feb. 1980.
10. Sajben, M., Kroutil, J. C., and Chen, C. P., "A High-Speed Schlieren Investigation of Diffuser Flows with Dynamic Distortion," AIAA Paper 77-0875, 1977.
11. Sajben, M., Kroutil, J. C., and Chen, C. P., "Unsteady Transonic Flow in a Two-Dimensional Diffuser," **Unsteady Aerodynamics**, AGARD CP 227, 1977, pp. 13-1 to 13-14.
12. Chen, C. P., Sajben, M., and Kroutil, J. C., "Shock-Wave Oscillations in a Transonic Diffuser Flow," **AIAA J.**, Vol. 17, Oct. 1979, pp. 1076-1083.

13. Sajben, M. and Kroutil, J. C., "Effects of Initial Boundary-Layer Thickness on Transonic Diffuser Flows," **AIAA J.**, Vol. 19, Nov. 1981, pp. 1386-1393.

14. Bogar, T. J., Sajben, M., and Kroutil, J. C., "Characteristic Frequencies of Transonic Diffuser Flow Oscillations," **AIAA J.**, Vol. 21, Sept. 1983, pp. 1232-1240.

15. Salmon, J. T., Bogar, T. J., and Sajben, M., "Laser Doppler Velocimeter Measurements in Unsteady, Separated, Transonic Diffuser Flows," **AIAA J.**, Vol. 21, Dec. 1983, pp. 1690-1697.

16. Sajben, M., Bogar, T. J., and Kroutil, J. C., "Forced Oscillation Experiments in Supercritical Diffuser Flows," **AIAA J.**, Vol. 22, April 1984, pp. 465-474.

17. Bogar, T. J., "Structure of Self-Excited Oscillations in Transonic Diffuser Flows," **AIAA J.**, Vol. 24, Jan. 1986, pp. 54-61.

18. Sajben, M. and Bogar, T. J., "Unsteady Transonic Flow in a Two-Dimensional Diffuser: Interpretation of Test Results," AFOSR-TR-83-0453, March 1982.

19. Wygnanski, W. and Petersen, R. A., "Coherent Motion in Excited Free Shear Layer Flows," AIAA Paper 84-0539, 1984.

20. Kibens, V. and Wlezien, R. W., "Active Control of Jets from Indeterminate Origin Nozzles," AIAA Paper 84-0542, 1984.

21. Reynolds, W. C. and Carr, L. W., "Review of Unsteady, Driven, Separated Flows," AIAA Paper 84-0527, 1984.

22. Wasserbauer, J. F. and Whipple, D. L., "Experimental Investigation of the Dynamic Response of a Supersonic Inlet to External and Internal Disturbances," NASA-TM-X-1648, 1968.

23. Bogar, T. J., Sajben, M., and Kroutil, J. C., "Response of a Supersonic Inlet to Downstream Perturbations," **J. Propul. Power**, Vol. 1, March-April 1985, pp. 118-125.

24. Sajben, M. and Crites, R. C., "Real-Time Optical Measurement of Time-Dependent Shock Position," **AIAA J.**, Vol. 17, Aug. 1979, pp. 910-912.

25. Roos, F. W. and Bogar, T. J., "Direct Comparison of Hot-Film Probe and Optical Techniques for Sensing Shock Wave Motion," **AIAA J.**, Vol. 20, Aug. 1982, pp. 1071-1076.

26. Culick, F. E. C. and Rogers, T., "The Response of Normal Shocks in Diffusers," **AIAA J.**, Vol. 21, Oct. 1983, pp. 1381-1390.

27. Atkins, H. L., "Comparisons and Applications of Time-Accurate Finite-Volume Methods for Solving the Unsteady Euler Equations," AIAA Paper No. 87-0189, January 1987.

28. Sajben, M., "The Propagation of Weak Compression Waves in Nonuniform Channel Flows," **J. Propul. Power** (accepted).

NOMENCLATURE

A	channel cross-sectional area
a	speed of sound
f	frequency
h	channel height
M	Mach number
p	pressure
R	perfect gas constant
T	temperature
t	time
w	wave speed
W	wave speed normalized with average sound speed
x	streamwise coordinate; x = 0. at throat
y	vertical coordinate; y = 0. at bottom wall
γ	ratio of specific heats
δ	boundary-layer thickness
θ	phase

Subscripts

e	exit station
o	plenum
t	total
tr	transducer
σ	shock
+	downstream-traveling
-	upstream-traveling
*	throat

Superscripts

$( )'$	ensemble-averaged pulse fluctuation value
$(\bar{})$	time-mean value

INITIAL DISTRIBUTION

16 Naval Air Systems Command
- AIR-4231 (1)
- AIR-5004 (2)
- AIR-522 (1)
- AIR-524 (1)
- AIR-536 (1)
- AIR-540 (1)
- AIR-5402 (1)
- AIR-5404 (1)
- AIR-93A (1)
- AIR-93D (1)
- AIR-9301B (2)
- AIR-932 (1)
- AIR-932G (1)
- PMA-242 (1)

6 Naval Sea Systems Command
- SEA-09B312 (2)
- SEA-521 (1)
- SEA-62R2 (1)
- SEA-62Z2 (2)

1 Space and Naval Warfare Systems Command (SPAWAR-005)
1 Commander in Chief, U.S. Pacific Fleet, Pearl Harbor (Code 325)
1 Commander, Third Fleet, San Francisco
1 Commander, Seventh Fleet, San Francisco
1 Air Test and Evaluation Squadron 5, China Lake
1 David Taylor Research Center, Bethesda (Code 166, J. Talbot)
3 Marine Corps Combat Development Center, Quantico (Landing Force Development Center)
1 Naval Air Development Center, Warminster (Code 3014)
1 Naval Explosive Ordnance Disposal Technology Center, Indian Head
1 Naval Ocean Systems Center, San Diego (Technical Library)
3 Naval Ordnance Station, Indian Head
- Code 5251 (1)
- Code 5253 (1)
- Technical Library (1)

2 Naval Research Laboratory
- Laboratory for Computational Physics
  - Dr. J. Gardner (1)
  - Dr. E. Oran (1)

1 Naval Strike Warfare, Fallon (Intelligence Library)
3 Naval Surface Warfare Center, White Oak Laboratory, Silver Spring
- Code K24 (1)
- Code R16 (1)
- Code R44, Dr. T. Hsieh (1)

2 Naval Technical Intelligence Center
- LNN, Liaison Officer (1)
- NITC-60, Library (1)

1 Naval War College, Newport
1 Pacific Missile Test Center, Point Mugu (Code 1094.7, P. McQuaide)
1 Army Armament Munitions and Chemical Command, Rock Island (DRSAR-LEM)
1 Army Ballistic Research Laboratory, Aberdeen Proving Ground (DRDAR-TSB-S (STINFO))
2 Air Force Systems Command, Andrews Air Force Base
- AFSC-SDZ (1)
- AFSC-XTTA (1)

6 Air Force Armament Division, Eglin Air Force Base
  AFATL/DLJG (1)
  AFATL/DLMA (1)
  AFATL/DLMI, Aden (1)
  AFATL/DLO (1)
  AFATL/DLODL (1)
  AFATL/FXE (1)
5 Air Force Astronautics Laboratory, Edwards Air Force Base
  Code MKCC (1)
  Code MKP (1)
  Technical Library (3)
1 Air Force Intelligence Agency, Bolling Air Force Base (AFIA/INTAW, MAJ R. Esaw)
5 Air Force Wright Aeronautical Laboratories, Wright-Patterson Air Force Base
  AFWAL/MLBT (3)
  AFWAL/POPR (1)
  AFWAL/POPT (1)
2 Foreign Technology Division, Wright-Patterson Air Force Base
  FTD/SDNW (1)
  FTD/TQFA (1)
1 Defense Advanced Research Projects Agency, Arlington
12 Defense Technical Information Center, Alexandria
1 Department of Defense Explosives Safety Board, Alexandria (6-A-145)
1 California Institute of Technology, Pasadena, CA (Prof. F. Culick)
1 Flow Research Company, Kent, WA (Dr. Wen-Huei Jou)
1 General Dynamics Corporation, Convair Division, San Diego, CA (Research Division)
1 General Dynamics Corporation, Pomona, CA (Via NAVPRO)
3 Georgia Institute of Technology, School of Aerospace Engineering, Atlanta, GA
  Prof. S. Lekoudia (1)
  Prof. W. Strahle (1)
  Prof. B. Zinn (1)
1 Grumman Aerospace Corporation, Bethpage, NY (TIC L01-35)
1 Honeywell Incorporated, Military Avionics Division, St. Louis Park, MN
1 Hudson Institute, Incorporated, Center for Naval Analyses, Alexandria, VA (Technical Library)
1 Hughes Aircraft Company, Missile Systems Group, Canoga Park, CA (Library)
1 Imperial College of Science and Technology, Department of Mechanical Engineering, London (Prof. J. Whitelaw)
3 McDonnell Douglas Corporation, St. Louis, MO
  Department E242, R. Fall (1)
  Dr. T. Bogar (1)
  Dr. M. Sajben (1)
1 Raytheon Company, Missile Systems Division, Bedford, Ma
1 Rockwell International Corporation, Missile Systems Division, Duluth, GA (F. Hessman)
1 San Diego State University, San Diego, CA (Prof. N. Nosseir)
2 Stanford University, Department of Mechanical Engineering, Stanford, CA
  Prof. C. Bowman (1)
  Prof. R. Hanson (1)
1 Teledyne-Ryan Aeronautical, San Diego, CA
1 The Boeing Company, Seattle, WA
1 The Johns Hopkins University, Applied Physics Laboratory, Laurel, MD (Kiersey)
1 United Technologies Corporation, Chemical Systems Division, San Jose, CA (T. Meyers)
1 United Technologies Research Center, East Hartford, CT (Document Control Station, R. O'Brien)
1 University of California, Berkeley, Department of Mechanical Engineering, Berkeley, CA (Prof. J. Daily)
1 University of California, Davis, CA (Prof. C. Law)
1 University of California, Irvine, Department of Mechanical Engineering, Irvine, CA (Prof. W. Sirignano)
1 University of Illinois, Department of Chemistry, Chicago, IL (Prof. R. Moriarity)
72 Chemical Propulsion Mailing List dated April 1985, including categories 1, 2, 3, 4, 5